JOURNAL OF AIRCRAFT
Vol. 44, No. 2, March–April 2007

Two-Dimensional Wind Tunnel and Computational Investigation of a Microtab Modified Airfoil

J. P. Baker,* K. J. Standish,† and C. P. van Dam‡
University of California, Davis, Davis, California 95616

DOI: 10.2514/1.24502

A computational and wind tunnel investigation into the effectiveness of a microtab-based aerodynamic load control system is presented. The microtab-based load control concept consists of a small tab, with a deployment height on the order of 1% of chord, which emerges approximately perpendicular to a lifting surface in the vicinity of the trailing edge. Lift mitigation is achieved by deploying the tabs on the upper (suction) surface of a lifting surface. Similarly, lift enhancement can be attained by tab deployment on the lower (pressure) surface of a lifting surface. A sensitivity analysis using Reynolds-averaged Navier–Stokes methods was conducted to determine optimal sizing and positioning of the tabs for active load control at a chord Reynolds number of 1.0×10^6 for the S809 baseline airfoil. These numerical simulations provide insight into the flow phenomena that govern this promising load control system and guided tab placement during the wind tunnel study of the S809 airfoil. The numerical and experimental results are largely in agreement and demonstrate that aerodynamic load control through microtabs is viable.

Nomenclature

C_d	=	section drag coefficient
C_l	=	section lift coefficient
C_{l_0}	=	section lift coefficient at $\alpha = 0$
$C_{l_{\max}}$	=	maximum section lift coefficient
$C_{l_{(L/D)_{\max}}}$	=	section lift coefficient for the $(L/D)_{\max}$ condition
c	=	chord length
D	=	drag
D'	=	drag per unit span
L	=	lift
$(L/D)_{\max}$	=	maximum section lift-to-drag ratio
M_∞	=	freestream Mach number
p	=	local pressure
p_∞	=	freestream pressure
q_{wake}	=	dynamic pressure in the wake
q_∞	=	freestream dynamic pressure
Re	=	chord Reynolds number
S_{exit}	=	exit plane
U_∞	=	freestream velocity
u	=	local velocity
u^*	=	friction velocity
y	=	wind tunnel coordinate in cross-flow (normal to wing plane) direction, or distance from the wall
y^+	=	local Reynolds number, yu^*/ν
α	=	angle of attack
$\alpha_{C_{l_{\max}}}$	=	angle of attack at $C_{l_{\max}}$
$\alpha_{(L/D)_{\max}}$	=	angle of attack at $(L/D)_{\max}$
ΔC_d	=	difference between the drag coefficient for a specified tab configuration and baseline
Δp	=	pressure difference in the wake, $p - p_\infty$
ν	=	kinematic viscosity
τ_{xx}	=	viscous stress

Presented as Paper 1186 at the 43rd AIAA Aerospace Sciences Meeting and Exhibit, Reno, NV, 10–13 January 2005; received 7 April 2006; accepted for publication 20 July 2006.

*Graduate Student Researcher, Department of Mechanical and Aeronautical Engineering. Student Member AIAA.

†Graduate Student Researcher, Department of Mechanical and Aeronautical Engineering; currently Engineer, GE Wind Energy.

‡Professor, Department of Mechanical and Aeronautical Engineering. Senior Member AIAA.

Introduction

ACTIVE load control for large wind turbine blades is being considered to maximize the energy capture of a rotor while keeping blade/rotor mass at a minimum. Techniques to control blade loads include blade pitch control, blade twist control, active servo flaps, active trailing-edge flaps or ailerons, and active translational microtabs [1–3]. The focus of this paper is on the microtab-based load control system. This system involves small tabs with a maximum deployment height on the order of the boundary-layer thickness, which are placed near the trailing edge of each turbine blade and deployed approximately normal to the surface (Fig. 1). Deployment of the tabs effectively changes the sectional camber of the rotor blade and the trailing-edge flow conditions, thereby altering the aerodynamic characteristics of the blade. One method for aerodynamic load control would use a variable height tab deployment system. Whereas this approach would allow for a continuous range of load control varying from full deployment to full retraction, the system would likely be difficult to design and expensive to manufacture and maintain. A much simpler on/off tab deployment system could be employed instead. As demonstrated by Mayda et al. [4], spanwise arrays of finite width tabs could be used to achieve a desired level of aerodynamic load control. The advantages of such a microtab concept are its low actuation power requirements, short actuation time, simplicity, and the fact that it requires minimal changes in current blade manufacturing techniques [1,2].

The purpose of this study is to present the experimental results and validate the computational fluid dynamics (CFD) methodology used to design and analyze the aerodynamic characteristics of the microtab-based load control technique. Also, the results of this experimental and computational investigation provide more information on the efficacy of two-dimensional microtabs for the S809 airfoil at a chord Reynolds number of 1.0×10^6. Static tabs are used as a precursor to active, translational tabs which will be studied in future work.

Computational Method

All of the calculations in this study were performed using the ARC2D flow solver [5] using the one-equation Spalart–Almaras [6] turbulence model. The code solves the compressible, two-dimensional Reynolds-averaged Navier–Stokes (RANS) equations in strong conservation-law form. The governing equations, in generalized curvilinear coordinates, are central differenced in standard second-order form and solved using the implicit Beam–

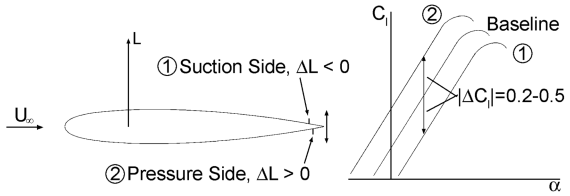

Fig. 1 Microtab-based aerodynamic load control concept.

Warming approximate factorization scheme [7]. Artificial dissipation terms are added for numerical stability with the second order dissipation coefficient equal to M_∞^3 and the fourth order dissipation coefficient set to 0.64. The code employs local time stepping and mesh sequencing to accelerate the convergence of steady solutions. Tripped-flow conditions were simulated by activating the turbulence model at the trip locations, which match those used in the wind tunnel experiment described next. ARC2D has been extensively applied to analyze inviscid and viscous flows over airfoils [5,8–10].

The primary grid generation tool used in this study is the Chimera Grid Tools (CGT) software package [11,12]. Traditional C-grids were used for each condition analyzed. The η-direction of the C-grid is defined to begin at the outflow boundary of the computational domain, in the wake of the airfoil, extending around the surface of the airfoil and finishing at the extent of the wake. The grid is then established in the direction of the outward normal, defined as the ξ-direction. The farfield of the grid was set at a distance of 50 chord lengths.

Grid spacing was initially established based on the turbulence model and spacing requirements about the trailing edge in the ξ-direction and η-direction, respectively. The initial grid spacing is necessary in the viscous flow regions, near the surface of the airfoil, but is computationally excessive in the inviscid regions. After initial spacing, the C-grid was smoothed to eliminate unnecessary points in the inviscid flow regions. In the η-direction, 300–450 surface points were used with stretching ratios of 1.05–1.2. The wake cut of the C-grid was defined by 75–100 grid points on either side. The initial grid spacing in the ξ-direction was specified by $y^+ \approx 1$. After smoothing, 125–150 grid points were used in the direction of the outward normal, with the first five points equally spaced and the latter points geometrically stretched. Grid refinement studies were conducted by doubling the grid density. The variation of grid densities produced negligible discrepancies in the results [13,14].

Experimental Approach

Wind Tunnel Facility

The aeronautical wind tunnel (AWT) at UC Davis is an open circuit, low turbulence wind tunnel manufactured by Aerolab [15]. The wind tunnel has test section area dimensions of 0.86×1.22 m (2.8×4 ft) and length of 3.66 m (12 ft). The test section is constructed with parallel sides, using four tapered fillets to compensate for boundary-layer growth and to preserve constant pressure throughout the section. The wind tunnel has low turbulence levels, less than 0.1% full scale for the initial 80% of the test section.

The wind tunnel test section contains two 0.91 m (36 in.) diameter turntables for the mounting of test apparatus. The first turntable is positioned over a six-component pyramidal balance, which can be connected to a model and used to measure aerodynamic forces (lift, drag, and side-force) and moments (roll, pitch, yaw). For a two-dimensional airfoil experiment, an airfoil model is fixed to the pyramidal balance such that the model bisects the test section vertically and extends from the floor to the ceiling (see Fig. 2).

Correction factors are used to account for the difference between unbounded and wind tunnel flows. The correction factors were determined for the S809 airfoil numerically using MSES [16] to account for wall interference effects including solid and wake blockage, and streamline curvature [17,18].

Whereas the balance adequately measures most forces and moments, previous experiments show that the pyramidal balance does not have the capability to accurately measure the drag force for a 2-D model. For this reason, a wake survey method has been implemented.

Fig. 2 A 2-D airfoil model, mounted in the UC Davis AWT test section.

Experimental Drag Determination

The wake survey method used in the AWT is based on momentum deficit in the wake of an object. Application of the conservation of momentum to a control volume around a body may be used to calculate the drag:

$$D = \int_{S_{\text{exit}}} [(p_\infty - p) + \tau_{xx} + (\rho_\infty U_\infty^2 - \rho u^2)]\,\mathrm{d}S \tag{1}$$

In Eq. (1), if we move the wake survey plane far downstream, the freestream pressure will equal the local pressure, and the viscous stress term will vanish. Under these conditions for two-dimensional incompressible flow,

$$D' = \int \rho u(U_\infty - u)\,\mathrm{d}y \tag{2}$$

which represents the drag per unit span of an airfoil.

Based on a method proposed by Jones [19], the drag of an airfoil can be determined by the evaluation of Eq. (2) at a single station in the wake. This method has been modified to use a three differential pressure transducer setup currently in use at the AWT. Each pressure transducer is a Setra Model 239 high accuracy, low-range pressure. The first transducer measures the freestream dynamic pressure. The second transducer measures the difference between the total and static pressures in the wake, q_{wake}, using a pitot-static probe of type PDD-24-G-21-KL manufactured by United Sensor Corporation. The final transducer measures Δp, the difference between the freestream pressure and the static pressure in the wake. According to Hopp [20], using the three differential pressure transducers, Eq. (2) can be represented as

$$C_d = 2\int \sqrt{\frac{q_{\text{wake}}}{q_\infty}}\left(1 - \sqrt{\frac{q_{\text{wake}} - \Delta p}{q_\infty}}\right)\mathrm{d}\left(\frac{y}{c}\right) \tag{3}$$

To experimentally determine the drag of an airfoil section, the pitot-static probe is moved across the exit plane in a step-stop fashion. The distance between flow measurements in the y-direction was set to 0.5 mm (0.02 in.). The tip of the pitot-static probe was fixed at one chord length downstream of the model trailing edge, at the tunnel center in the spanwise direction. Several spanwise measurements were made to validate the 2-D flow assumption. Little spanwise variation was found in the center 75% span region of

the airfoil. The discrepancies increased beyond statistical levels as the pitot-static probe approached 0.08–0.1 m (3–4 in.) away from the ceiling and floor of the test section. Because the flow is 2-D, only one traverse through the plane at a given position with respect to the span of the airfoil is necessary. According to Eq. (3), the integrand contributes to the drag only in the disturbed portion of the wake; thus, only this region of the test section need be analyzed. Further information concerning the AWT test facility may be found in [20–22].

Test Procedure

The S809 airfoil is a 21% thick airfoil designed by NREL for applications with stall-controlled horizontal-axis wind turbines [23]. The current study involves modifying a nominal S809 two-dimensional airfoil model with brass L-shaped brackets at various locations along the upper (suction) and lower (pressure) surfaces. The L-brackets were affixed to the airfoil using double-sided tape manufactured by 3M (Removable, Repositionable Tape 666), with an average thickness of 0.05 mm (0.002 in.).

The airfoil study was conducted at a Reynolds number of 1.0×10^6, under both free and fixed transition conditions. Fixed transition was ensured using zigzag trip strips placed on the upper and lower surfaces at 2% chord and 5% chord (as measured from the leading edge), respectively. The trip location was chosen to match test methods employed by Somers [23]. The trip sizing was determined based on methods by Braslow and Knox [24] using a roughness Reynolds number of 600. Based on these methods, zigzag tape heights of 0.25 and 0.4 mm were selected for use on the upper and lower surfaces, respectively. Tab location studies were conducted using a tab height (TH) of 1.1% chord at 90, 95, and 100% chord on the pressure (lower) surface, and at 40, 60, 90, and 100% chord on the suction (upper) surface. A tab height survey was conducted on the suction and pressure surfaces at 90 and 95% chord locations, respectively, using tabs heights of 1.1, 1.6, and 2.2% chord.

Uncertainty Analysis

A detailed uncertainty analysis for the two-dimensional experimental results from the AWT has been performed using methods described in [25,26]. The results of this analysis described here are a summary of information from Hopp [20], Zayas [21], and Baker [22]. For the purposes of this paper, the resultant quantities described are the lift and drag coefficients, as well as the Reynolds number. For the sake of brevity, typical measured values will be presented accompanied by an estimate of uncertainty at 95% confidence.

The details of the analysis for lift and Reynolds number are discussed at length in Hopp [20] and Zayas [21]. For a Reynolds number of 1.0×10^6, an uncertainty of approximately 6400, or 0.64%, was determined. For a lift coefficient measurement of 0.5912, an uncertainty of 0.00565, or 0.96%, was determined.

The complexity of the equation for the drag coefficient, given by Eq. (3), requires numerical methods for a complete analysis. For this reason, a Monte Carlo simulation was used to determine the uncertainty in drag, as detailed in Baker [22]. From [22], it was determined that the uncertainty in drag is highly dependent on the condition of the wake. For instance, larger, more unsteady wakes will produce greater uncertainty in drag. Thus, the uncertainty of the drag at 0 and 10 deg for the baseline S809 airfoil are presented for reference. The uncertainty in drag is also dependent on flow angularity because of its influence on the bias error of the pitot-static pressure measurements. For minimal angularity, pitot-static uncertainty may be as low as 0.01% [17]. Neglecting pitot-static bias, at 0 deg angle of attack, the drag coefficient was determined to be 0.01008 with an uncertainty of 0.00026, or 2.5%. For the baseline S809 airfoil at 10 deg, the drag coefficient was determined to be 0.02666 with an uncertainty of 0.00046, or 1.7%.

Experimental Results

In this section experimental results are presented for the S809 airfoil at $Re = 1.0 \times 10^6$, modified by static tablike devices using L-shaped brackets. The effects of tabs placed on the upper and lower surfaces at various heights and locations have been experimentally determined. The experimental results were obtained at free and fixed boundary-layer transition conditions.

Experimental Validation

The S809 airfoil was first experimentally investigated by Somers [23] in 1986. The baseline S809 airfoil model was studied for free and fixed transition at $Re = 1.0 \times 10^6$ and compared to the results published by Somers. The free and fixed transition results are shown in Figs. 3 and 4, respectively. The lift curves for free and fixed transition are shown in Figs. 3a and 4a. Both figures show slight deviation between the present study and Somers at negative angles of attack, and slight deviation between 5 and 9 deg. The discrepancies may be due to physical differences in the models used for the present study and Somers, e.g., trailing-edge thickness variation, or surface roughness. Despite the slight deviations, Figs. 3a and 4a demonstrate consistent increments in lift between the free and fixed transition conditions for both the present study and Somers. The drag polars for free and fixed transition are shown in Figs. 3b and 4b. The free transition drag polars agree well with Somers, with the exception of the aforementioned lift discrepancies near $C_l = 0.8$–0.9. For fixed

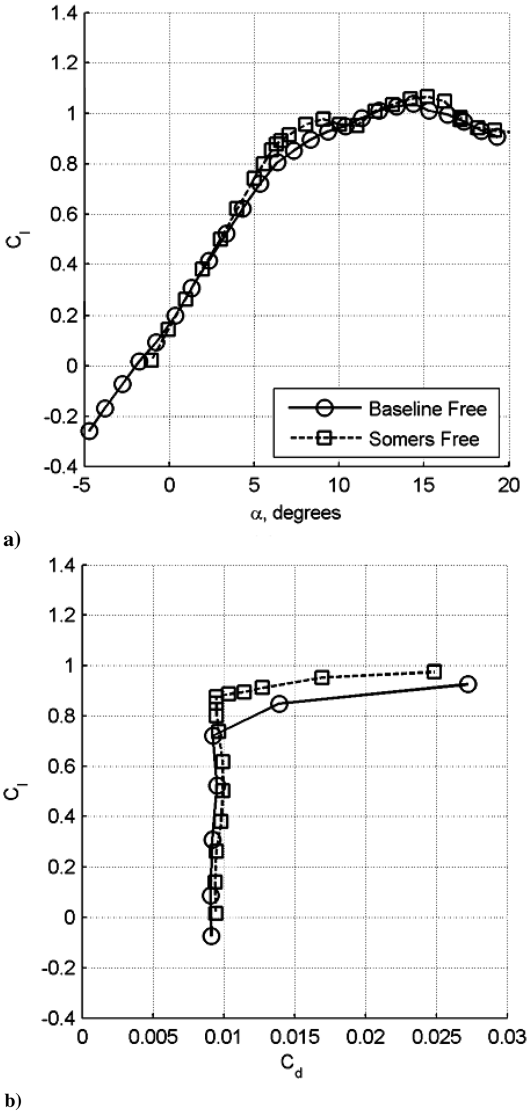

Fig. 3 Comparison of current study to Somers [23], free transition: a) lift curve and b) drag polar.

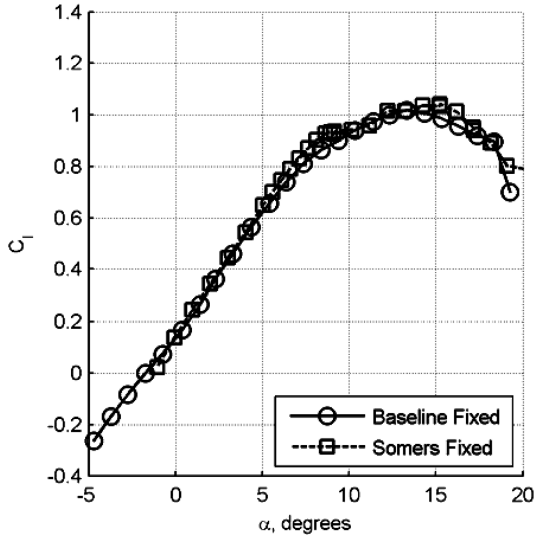

a)

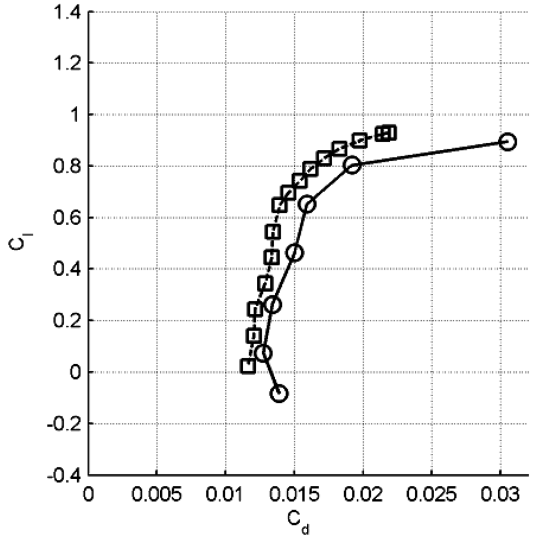

b)

Fig. 4 Comparison of current study to Somers [23], fixed transition: a) lift curve and b) drag polar.

transition, the present drag values are consistently higher, by 10%–15%, than those reported by Somers. The higher fixed transition drag values are possibly due to differences in trip methods between the present study using zigzag trip tape and Somers using distributed grit.

Lower Surface Tab Study (Free Transition)

The lower surface tab studies conducted at $Re = 1.0 \times 10^6$ under free transition conditions may be separated into tab location and tab height surveys. The tab location survey was conducted on the lower surface using a 1.1% chord tab height at the following locations: trailing edge (TE), 95% chord, and 90% chord. The tab height survey involved placing a tab at 95% chord and using tab heights of 1.1, 1.6, and 2.2% chord. A summary of lower surface tab results in terms of several pertinent airfoil performance parameters is presented in Table 1. "LTL" designates the lower (pressure) surface tab location.

Tab Location

The chordwise tab location survey results are presented in Fig. 5. Figure 5a shows the lift coefficient as a function of angle of attack. As shown, the lift curve including maximum lift is affected by the tab. The general trend indicates that tabs placed aft of 95% chord on the lower surface increase maximum lift, accompanied by a positive shift in the lift curve. The tabs are most effective when located at the trailing edge. Marked increases in lift can be achieved, however, using tabs placed forward of the trailing edge. Interestingly, it appears that positioning the tabs too far forward along the lower surface can result in a reversal of this effect, as seen for the 90% chord tab configuration with lift loss for $\alpha > 6$ deg.

Table 1 Experimental results for baseline and airfoil modified by lower (pressure) surface tabs, free transition

LTL	TH	C_{l_0}	$C_{l_{\max}}$	$\alpha_{C_{l_{\max}}}$	$(L/D)_{\max}$	$C_{l_{(C/D)_{\max}}}$	$\alpha_{(L/D)_{\max}}$
——	——	0.165	1.038	14.39	78.1	0.721	5.35
TE	1.1%	0.438	1.255	12.34	68.7	1.021	5.34
95%	1.1%	0.279	1.111	13.40	63.7	0.861	5.35
95%	1.6%	0.357	1.192	13.37	63.7	0.945	5.35
95%	2.2%	0.436	1.239	12.30	56.9	1.020	5.33
90%	1.1%	0.193	0.934	14.38	55.5	0.732	5.34

The loss of lift for the 90% chord tab configuration may be explained by flow reattachment before the trailing edge [13,14]. For a given tab height, it is possible to place a tab far enough ahead of the trailing edge such that as the angle of attack is increased, the localized flow separation due to the tab is not sustained with the flow reattaching ahead of the trailing edge of the airfoil. This reattachment eliminates the Kutta condition shift [13,14] and results in a loss in lift due to the tab-generated separation bubble. The possibility of flow reattachment limits the distance from the trailing edge for lower surface tabs of a given height.

The lift-enhancing characteristics of pressure surface tabs does not come without penalty. Figure 5b shows the effect of lower surface tabs on the drag coefficient. The baseline S809 airfoil is a low-drag airfoil and, hence, adding a tab does increase the drag. For equal tab height, the drag does not seem to be affected by tab location on the lower surface for angles of attack below incipient stall. In fact, a fairly uniform increase in drag of approximately 37 drag counts is observed in the linear lift regime. As the angle of attack approaches maximum lift, positioning the tabs closer to the trailing edge tends to improve the lift-to-drag performance.

Tab Height

The effect on lift coefficient for varying tab height for tabs placed on the pressure surface at 95% chord is shown in Fig. 6a. Increasing tab height tends to augment the lift-enhancing effects of tabs placed on the lower surface. The 2.2% chord tab placed at 95% chord has a very similar $C_{l_{\max}}$ to the 1.1% chord tab placed at the trailing edge (see Fig. 5). Figure 6b, however, shows increasing the tab height causes a significant increase in drag, suggesting the existence of a combination of tab height and chordwise location that optimizes the lift-to-drag ratio [2].

Upper Surface Tab Study (Free Transition)

Similar to the lower surface tab study, the upper surface study conducted at $Re = 1.0 \times 10^6$ under free transition conditions is separated into tab location and height surveys. The tab location survey was conducted on the upper surface using a tab 1.1% chord in height placed at the trailing edge, 90% chord, 60% chord, and 40% chord. The forward locations (60 and 40% chord) were selected based on CFD simulations [13] that indicated a beneficial effect (i.e., lift reduction) of forward tab locations on the upper surface. For the tab height survey, tabs were placed at the 90% chord location using 1.1, 1.6, and 2.2% chord heights. A summary of upper surface tab results in terms of several pertinent airfoil performance parameters is presented in Table 2. "UTL" designates the upper (suction) surface tab location.

Tab Location

The upper surface chordwise tab location survey results are presented in Fig. 7. As shown in Fig. 7a, placing tabs on the upper surface has a mitigating effect on lift; the lift curve is shifted downward dependent on the placement of the tabs. The trailing edge and 90% chord location tabs have similar lift behavior. Both tab

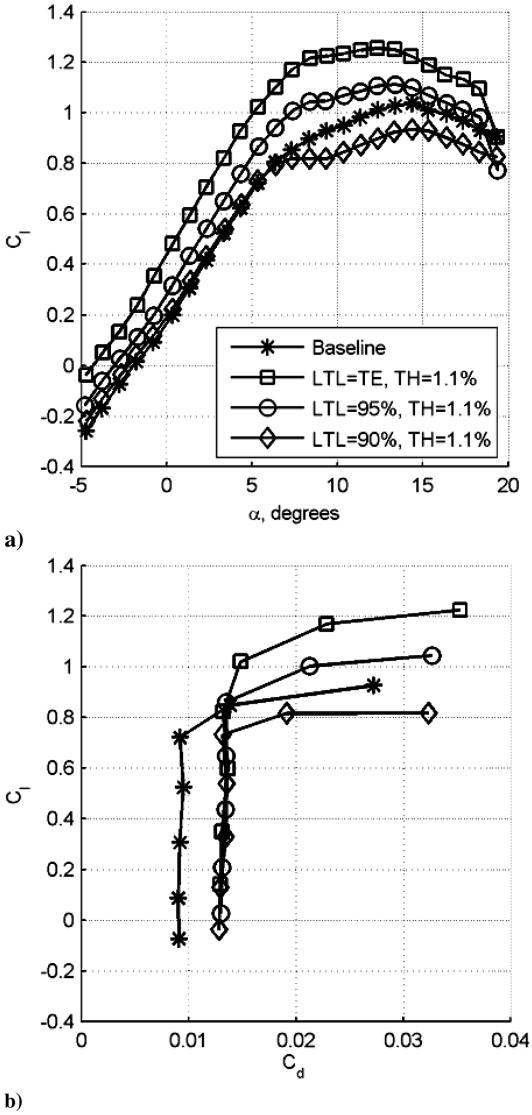

Fig. 5 Tab location study, lower (pressure) surface tab, free transition: a) lift curve and b) drag polar.

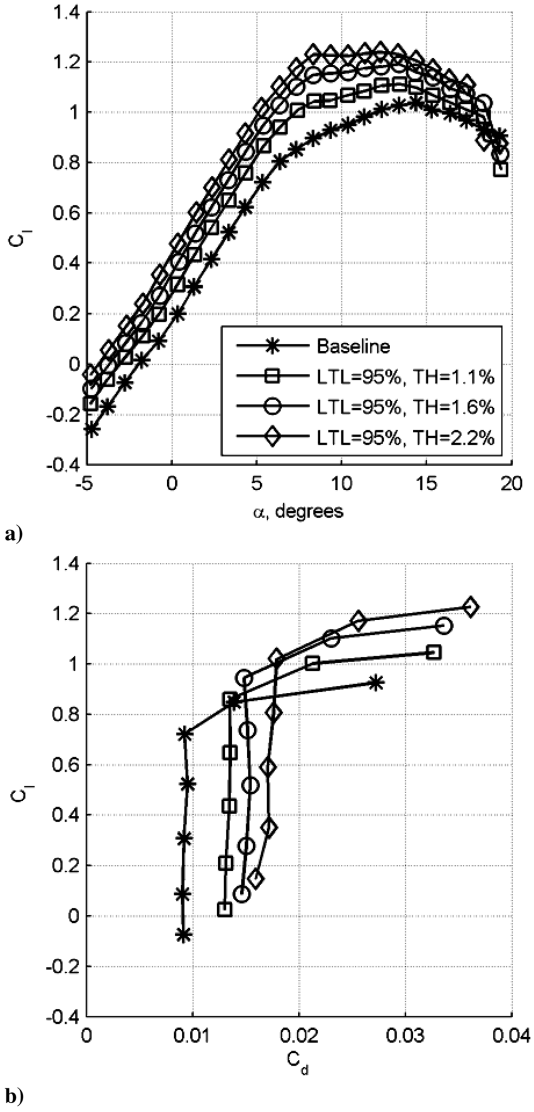

Fig. 6 Tab height study, lower (pressure) surface tab, free transition: a) lift curve and b) drag polar.

locations shift the linear portion of the lift curve, for example, the measured C_l of 0.54 for the tab modified airfoil compared to the baseline C_l of 0.72 at $\alpha = 5$ deg, and lose effectiveness at angles of attack around 8 deg. The loss of effectiveness is defined by the incidence angle at which the baseline and tab modified airfoil have nearly corresponding lift values. The 60% chord tab location causes a shift in the lift curve and a reduction in its slope, but loses effectiveness at approximately 11.5 deg. The 40% chord tab location causes a slightly different lift behavior. Following the lift curve from negative to positive angles of attack (left to right), this case appears to affect the lift curve almost identically to the 60% chord case until the angle of attack reaches 0 deg, where a marked decrease in lift occurs until losing effectiveness at around 16 deg.

The loss of effectiveness for tabs placed on the upper surface may be explained by the trailing-edge stall characteristics of the S809 airfoil at this Reynolds number [23]. The flow separation region continues to grow with increasing angle of attack. Thus, as the flow separation grows and moves forward, the tabs are engulfed in separated flow and lose effectiveness. This may explain why the loss of effectiveness appears to occur so suddenly for each of the tab configurations in Fig. 7a. This also explains why tabs placed further forward on the airfoil surface maintain lift mitigating capabilities until higher angles of attack.

Figure 7b shows the drag penalty of placing tabs on the suction surface of the airfoil. As shown, moving the tabs forward causes an increase in drag. For the 60 and 40% chord cases, this increase in drag is substantial. Placing tabs at the trailing edge and 90% chord locations increases the drag by approximately 45 and 65 drag counts over baseline, respectively.

Tab Height

Figure 8a shows that increasing the tab height at a fixed location of 90% chord along the upper surface tends to improve the lift mitigation effect. For instance, doubling the tab height from 1.1 to 2.2% chord, improves mitigation of lift by yielding a C_l of 0.54 and 0.42 for the 1.1 and 2.2% chord tab heights, respectively, compared to the baseline C_l of 0.72 at $\alpha = 5$ deg. It is also clear, however, that increasing tab height does not significantly improve the effective angle of attack range of the tab. Each of the three tab heights

Table 2 Experimental results for baseline and airfoil modified by upper (suction) surface tabs, free transition

UTL	TH	C_{l_0}	$C_{l_{\max}}$	$\alpha_{C_{l_{\max}}}$	$(L/D)_{\max}$	$C_{l_{(C/D)_{\max}}}$	$\alpha_{(L/D)_{\max}}$
——	——	0.165	1.038	14.39	78.1	0.721	5.35
TE	1.1%	−0.020	1.050	14.32	50.8	0.812	7.31
90%	1.1%	0.009	1.039	14.37	43.4	0.764	7.37
90%	1.6%	−0.040	1.048	14.37	38.8	0.723	7.35
90%	2.2%	−0.103	1.055	14.36	33.7	0.668	7.33
60%	1.1%	0.080	1.025	14.32	18.2	0.792	9.28
40%	1.1%	0.057	0.997	16.34	4.0	0.489	9.27

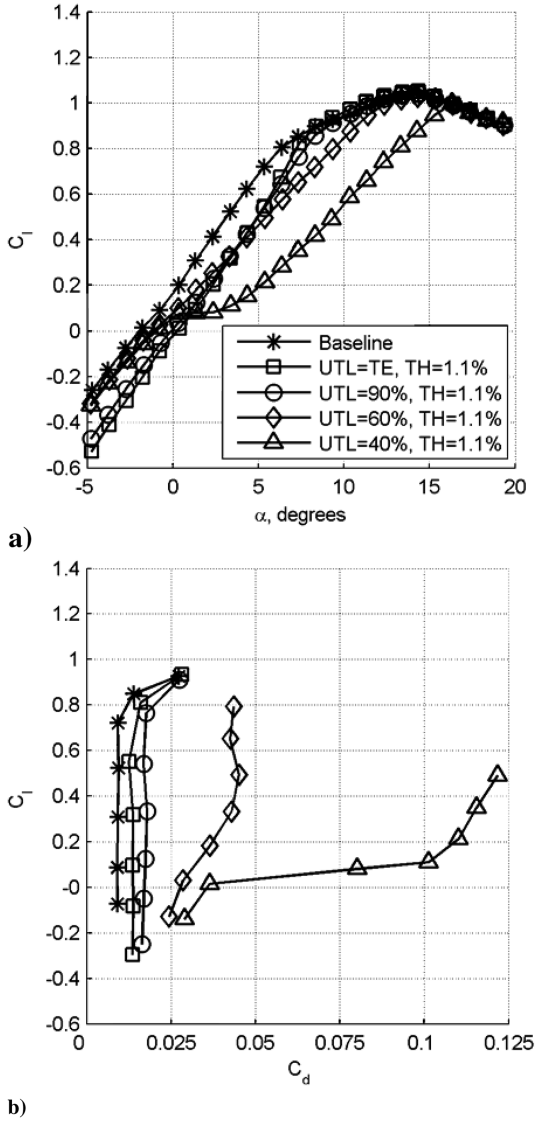

Fig. 7 Tab location study, upper (suction) surface tab, free transition: a) lift curve and b) drag polar.

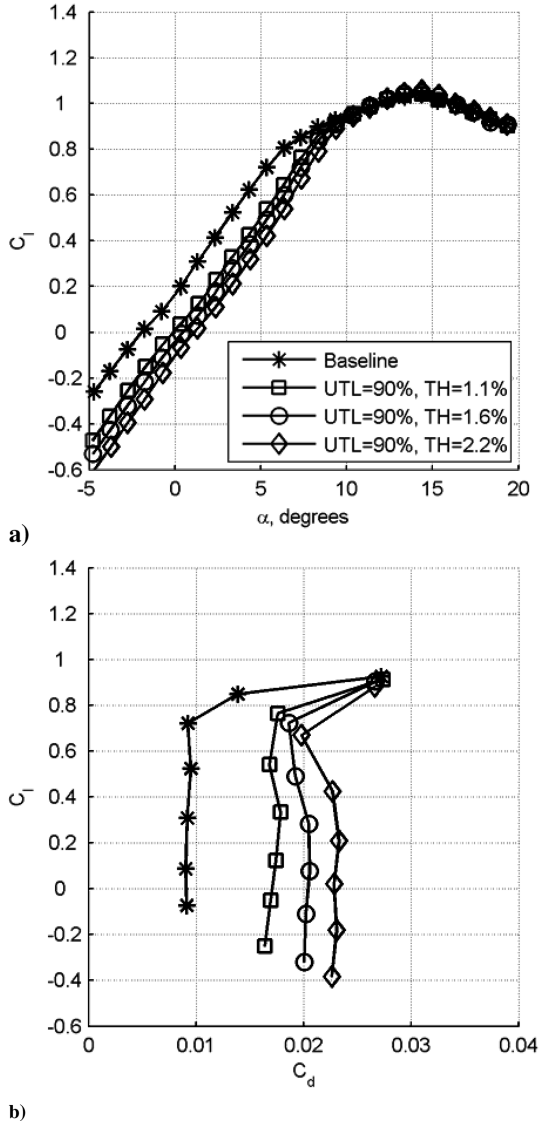

Fig. 8 Tab height study, upper (suction) surface tab, free transition: a) lift curve and b) drag polar.

investigated (1.1, 1.6, and 2.2% chord) lose effectiveness at nearly the same angle of attack (around 8 deg).

Figure 8b shows increasing tab height causes a marked increase in drag, until the tabs are overcome by flow separation. For example, doubling the tab height from 1.1 to 2.2% chord increases the drag from 70 to 130 drag counts over the baseline airfoil.

Upper and Lower Tab Study (Fixed Transition)

Because of the possibility of tripped-flow conditions in real-world applications, which may occur due to dirty or rough leading edges, the effects of tripped flow on tab effectiveness was measured. It is also desirable to study tripped-flow conditions because of the lack of transition prediction capabilities in many current Reynolds-averaged Navier–Stokes methods, including ARC2D. Adequate comparisons between CFD and experiment require similar initial conditions, such as transition location.

The tripped-flow study was conducted using a baseline airfoil modified with zigzag trip devices placed on the upper and lower surfaces at 2 and 5% chord locations, respectively. The tripped baseline airfoil was then modified by placing a 1.1% chord L-bracket on the upper and lower surfaces. The lower surface tab was placed at 95% chord. Tabs were placed at 90 and 60% chord locations on the upper surface.

The effects of tripped flow on the lift characteristics of the tab modified S809 airfoil are shown in Figs. 9 and 10. For comparison, Figs. 9 and 10 also include the corresponding free transition configurations. As shown in Fig. 9a, tripping the boundary layer near the leading edge decreases the lift values of the baseline airfoil for all angles of attack. This trend is similarly repeated for the S809 airfoil modified with tabs, see Figs. 9a and 10a. Tripping the flow does not seem to adversely affect the ability of the tabs to increment the lift of the S809 airfoil.

Figures 9b and 10b show the influence of tripping the flow on drag. As shown, the boundary-layer trips cause an increase in drag over the free transition cases. This is to be expected because of an increase in skin friction and form drag resulting from the earlier onset of turbulent flow. The upper surface 60% chord configuration, however, presents an interesting divergence from this trend. Figure 10b shows that the tripped-flow 60% chord tab case actually has lower drag than its free transition counterpart for higher lift coefficients. This may be due to the earlier onset of turbulence for the tripped-flow configuration resulting in increased boundary-layer thickness at the tab location. The increased boundary-layer thickness causes a given tab height to have less influence on drag.

Comparison of Computational and Experimental Results

Because of the lack of a transition model in the RANS method used here, comparison of the CFD results to experiment are limited to

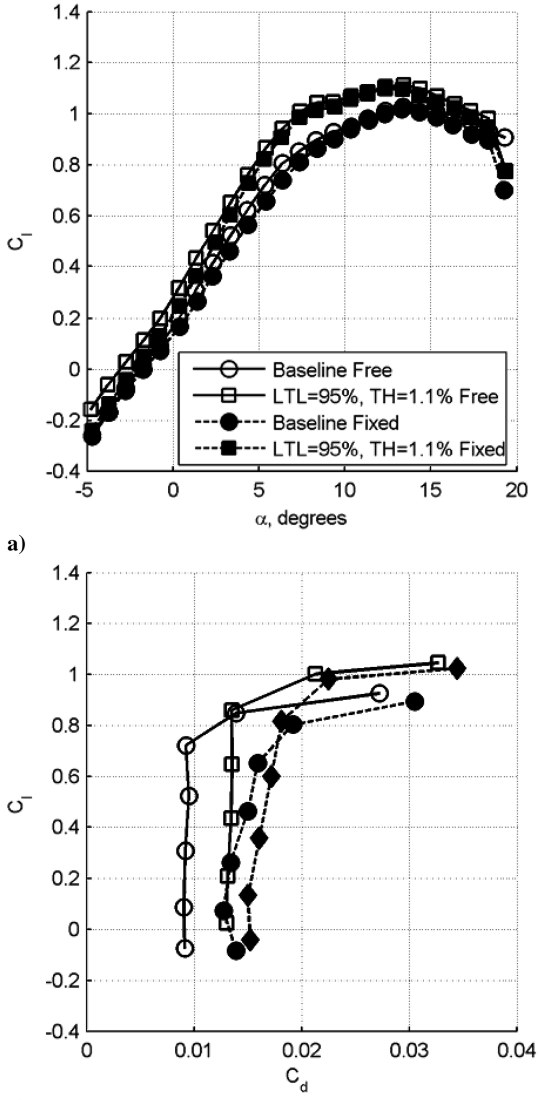

Fig. 9 Comparison of fixed and free transition for baseline and airfoil with lower (pressure) surface tab: a) lift curve and b) drag polar.

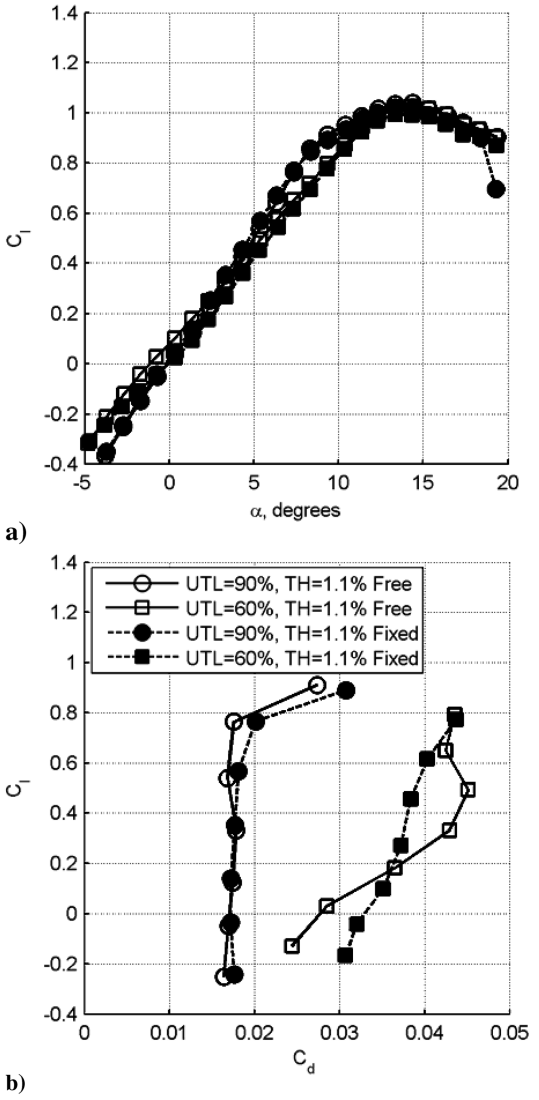

Fig. 10 Comparison of fixed and free transition for baseline and airfoil with upper (suction) surface tab: a) lift curve and b) drag polar.

fixed transition conditions. The complete CFD study for the S809 airfoil is published by Standish [13]. A comparison of computational and experimental results for a nominal tab height of 1% chord may be found in Figs. 11–13. Figures 11a and 12a show the lift coefficient vs angle of attack and demonstrate fair agreement between computational and experimental values, especially in the linear lift regime. Near stall, disagreement between the data is shown. This disagreement is expected because of limitations in turbulence modeling in the numerical simulations and difficulties modeling unsteady, three-dimensional effects with massive flow separation and difficulty in obtaining valid experimental data for highly separated flows. Discrepancies may also exist due to the tab height difference between experiment (1.1% chord) and computation (1.0%). For the 60% chord configuration (Fig. 12a), much of the upper surface experiences separated flow, which explains the deviation between computational and experimental results. The same general trends exist for drag, as shown in Fig. 11b and 12b.

Because the goal of the microtab system is load control, the effectiveness of the tabs may be demonstrated by plotting the deviation of a microtab configuration from the baseline condition. This method is also helpful in illustrating the ability of CFD to match the trends found in experiment, or vice versa, as demonstrated for the linear lift regime in Fig. 13a. As shown, fair agreement between experiment and CFD exists for the overall trends for each of the microtab configurations. Figure 13a demonstrates that CFD accurately predicts the behavior of the 60% chord configuration even when separated flow exists.

The drag due to the tab may also be predicted by CFD and validated by experiment, as demonstrated in Fig. 13b. The predicted drag increments are in good agreement except for the 60% chord configuration where the overall trend is captured but the increment in drag is underpredicted by CFD. The discrepancy in drag increment for the 60% chord configuration may be due to unsteady flow phenomena that are inaccurately modeled by the computational method.

Discussion

The microtab has been proposed as a novel load control method for airfoils. The proposed method involves sliding small-scale tabs, on the order of 1% chord, perpendicularly out of the surface of the airfoil to prevent problems associated with hinge-type devices. Because the tabs will slide in and out of the surface, a volume constraint is imposed precluding the use of the trailing edge as a viable candidate for tab location. Thus, a tab location forward from the trailing edge is required.

Placing tabs on the lower (pressure) surface produces a lift increment, which is most appreciable for larger tab heights and tabs placed closer to the trailing edge. The trailing-edge tab has the greatest effect on lift for a given tab height. Moving the tab forward somewhat diminishes this effect, but substantial increases in lift can

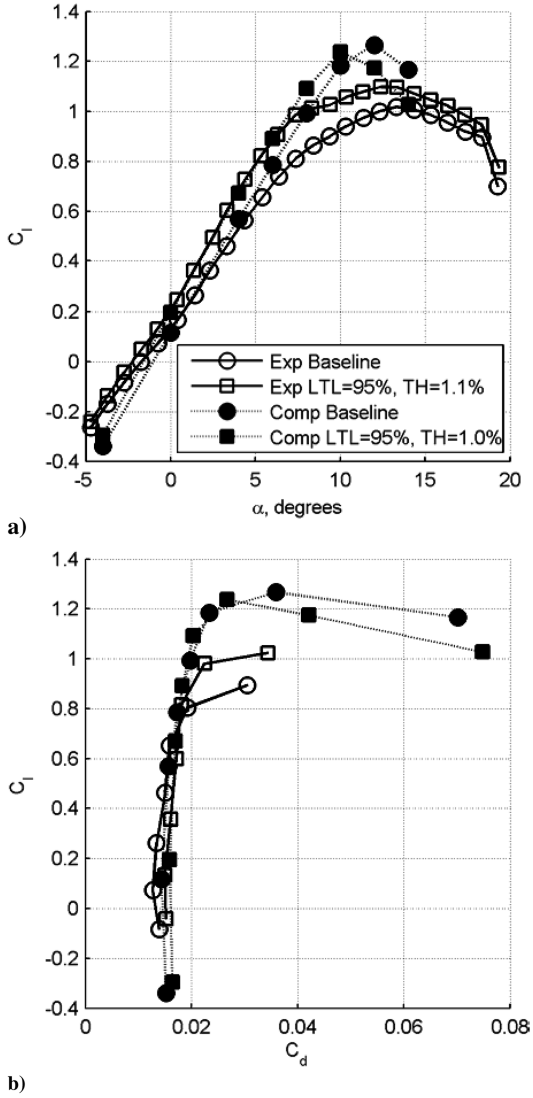

Fig. 11 Comparison of computational and experimental results for baseline airfoil with lower surface tab, fixed transition: a) lift curve and b) drag polar.

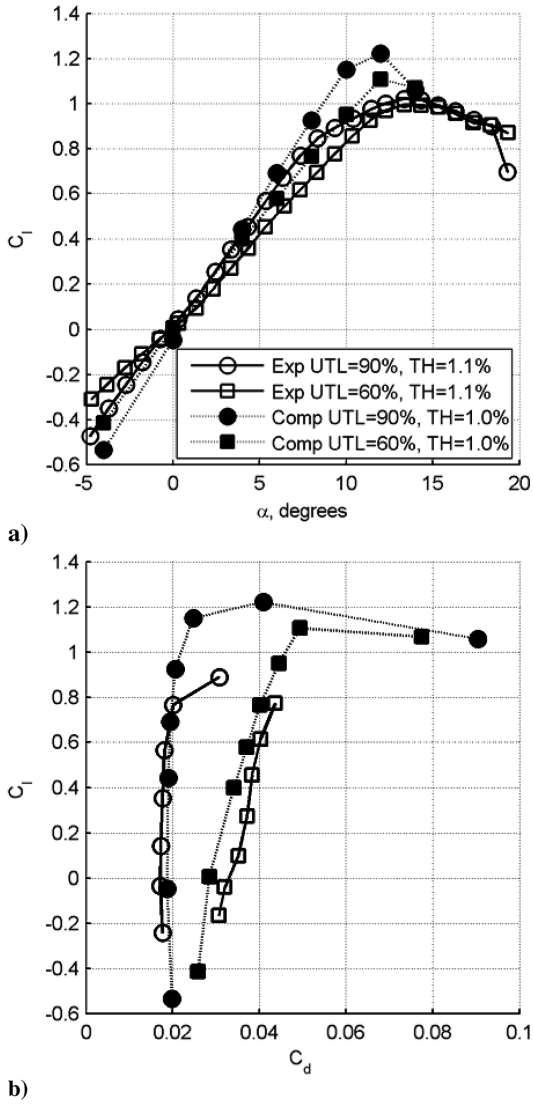

Fig. 12 Comparison of computational and experimental results for baseline airfoil with upper surface tab, fixed transition: a) lift curve and b) drag polar.

still be achieved. It is possible, however, to move the tab too far forward, in which case a reversal of this trend may occur. Thus, careful selection of tab location must be made. Before stall, the drag for the airfoil with lower surface tabs was insensitive to tab location. After the onset of stall, the drag for airfoils with lower surface tabs was found to increase as the tabs were moved further aft. Increasing the tab height can also be used to cause a positive shift in the lift curve and increase the maximum lift of the S809 airfoil. Increasing the tab height, however, causes an increase in drag. Thus, an optimum tab location and height may be found that maximizes lift increases while minimizing the drag penalty, as shown in Fig. 14.

Placing tabs on the upper (suction) surface has the opposite effect: lift is mitigated. The effectiveness of the tab is lost once the flow separation region reaches the chordwise location of the tab. Placing the tab further forward along the upper surface (60 and 40% chord locations) tends to prolong its effectiveness to higher angles of attack. It was found that tabs further aft (90% and TE chord locations), however, tend to have a greater lift mitigating effect for $-5 < \alpha < 2$ deg. These findings indicate that the application for which these tabs may be used has to be analyzed to determine the desired angle of attack regime. If full range of motion is desired, perhaps several chordwise tab locations spaced appropriately over the upper surface can be used. Increasing tab height along the upper surface tends to improve the lift mitigation at the expense of substantial increases in drag, as shown in Fig. 15.

Understanding the effects of fixed transition on tab performance is important for comparison between experimental and CFD results. It is also important for applications in which fixed transition is desirable or expected to occur. Comparison of the free and fixed transition results show that the tab effectiveness is nominally unchanged for the configurations and conditions studied here.

A combination of computational fluid dynamics and experimentation has been used to effectively design microtab-based load control devices for the S809 airfoil. In this study, computational results were used to conduct sensitivity analyses to determine appropriate tab configurations for further investigation and validation. This approach has saved both time and resources by limiting the number of test configurations necessary for experimental analysis.

Conclusions

The proposed microtab concept for active load control of airfoils is based upon small tabs (approximately 1% chord) that emerge from a lifting surface approximately perpendicular to its surface, similar to a Gurney flap, yet well ahead of the trailing edge. Deployment of a tab on the lower surface, in the vicinity of the trailing edge, has been shown to be an effective means of lift enhancement. Similarly, lift mitigation can be achieved by tab deployment on the upper surface within the pressure recovery region.

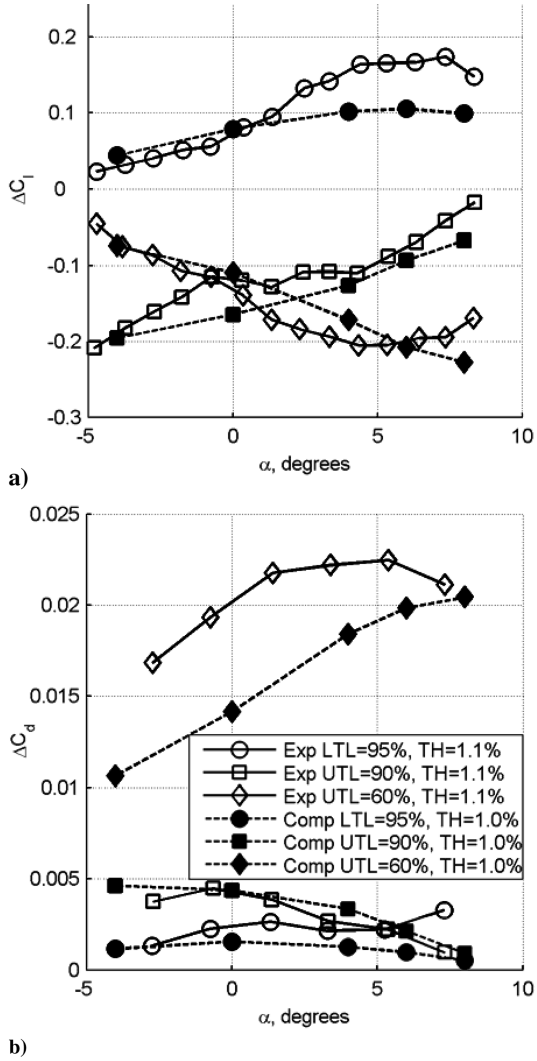

Fig. 13 Comparison of computed and measured tab effects on a) lift and b) drag, fixed transition.

The computational and experimental results of the lower (pressure) surface tab effectiveness study indicate that the optimal tab location for lift enhancement is at the trailing edge because this location provides a maximum lift increment for a minimal drag penalty. The trailing-edge location, however, does not provide sufficient structural volume to house the retracted tab and actuation device. Therefore, the optimal tab location is likely to exist as far aft as the volume requirements will permit. The optimal tab height is likely to be on the order of the boundary-layer thickness, or perhaps slightly larger to account for the location ahead of the trailing edge.

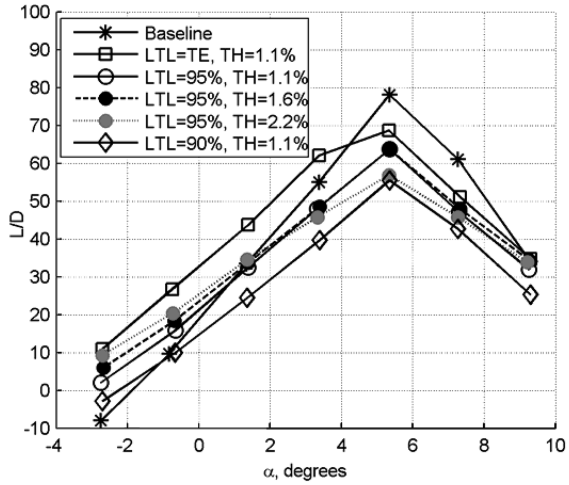

Fig. 14 C_l/C_d vs α for the lower (pressure) surface tab configurations, free transition.

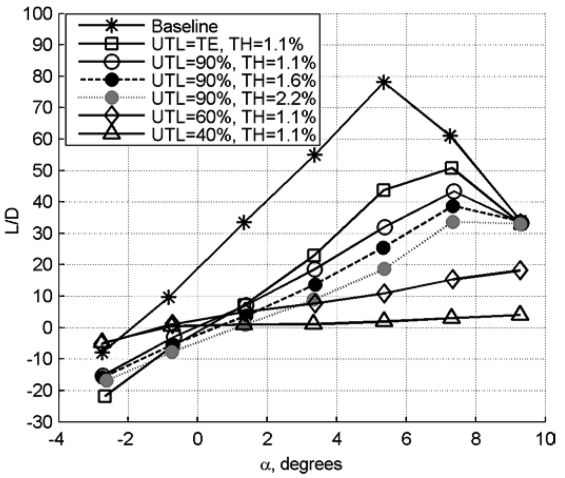

Fig. 15 C_l/C_d vs α for the upper (suction) surface tab configurations, free transition.

The computational and experimental results of the upper (suction) surface tab effectiveness study indicate that selecting the optimal tab location for lift mitigation is more complicated. The optimal location for lift mitigation has a greater dependence on the geometric and aerodynamic characteristics of the baseline airfoil, as well as the application and anticipated flow conditions. The results indicate that for lift coefficients near stall, the optimal tab location for lift mitigation is as far forward from the trailing edge as possible while remaining within the pressure recovery region. On the other hand, in the linear lift regime, the pressure gradient on the upper surface is not significant enough to sustain separated flow between the forward tab locations and the trailing edge. Under these conditions, the optimal tab location for lift mitigation is as far aft as the volume requirements will permit. It should also be noted that although the forward tab locations provide the most significant lift mitigation for moderate to high lift coefficients, they also provide higher drag penalties. Therefore, the optimal tab location depends on the application, expected operating conditions, and the tradeoff between increased lift mitigation at the expense of increased drag.

The results of this study demonstrate that careful analysis of tab height and location, combined with the selection and/or design of an appropriate baseline airfoil, can yield an effective active load control system. Future efforts will focus on the unsteady load variations that occur during tab deployment and retraction, spanwise load variations as a result of tab placement and tab gaps, and the development of a proof of concept, including microtab actuators, sensors, and control system, to validate and demonstrate the load control capabilities of this type of system.

Acknowledgments

This work is supported by the Wind Energy Technology group of the Sandia National Laboratories, Albuquerque, New Mexico. Additional funding was received from Lawrence Livermore National Laboratory.

References

[1] Yen, D. T., van Dam, C. P., Bräeuchle, F., Smith, R. L., and Collins, S. D., "Active Load Control and Lift Enhancement Using MEM Translational Tabs," AIAA Paper 2000-2422, June 2000.

[2] Yen-Nakafuji, D. T., van Dam, C. P., Smith, R. L., and Collins, S. D., "Active Load Control for Airfoils Using Microtabs," *Journal of Solar Energy Engineering*, Vol. 123, Nov. 2001, pp. 282–289.

[3] Chow, R., and van Dam, C. P., "Unsteady Computational Investigations of Deploying Load Control Tabs," *Journal of Aircraft*, 2006 (in print).

[4] Mayda, E. A., van Dam, C. P., and Yen-Nakafuji, D., "Computational Investigation of Finite Width Microtabs for Aerodynamic Load Control," AIAA Paper 2005-1185, Jan. 2005.
[5] Pulliam, T. H., "Efficient Solution Methods for the Navier-Stokes Equations," *Lecture Notes for the von Kármán Institute for Fluid Dynamics Lecture Series: Numerical Techniques for Viscous Flow Computation in Turbomachinery Bladings*, von Kármán Institute, Rhode-St-Genese, Belgium, 1985.
[6] Spalart, P. R., and Allmaras, S. R., "A One-Equation Turbulence Model for Aerodynamic Flows," *La Recherche Aérospatiale*, No. 1, 1994, pp. 5–21.
[7] Beam, R., and Warming, R. F., "An Implicit Finite-Difference Algorithm for Hyperbolic Systems in Conservation Law Form," *Journal of Computational Physics*, Vol. 22, Sept. 1976, pp. 87–110.
[8] Chao, D. D., and van Dam, C. P., "Airfoil Drag Prediction and Decomposition," *Journal of Aircraft*, Vol. 36, No. 4, July–Aug. 1999, pp. 675–681.
[9] Barth, T. J., Pulliam, T. H., and Buning, P. G., "Navier-Stokes Computations for Exotic Airfoils," AIAA Paper 85-0109, Jan. 1985.
[10] Zingg, D. W., "Low Mach Number Euler Computations," *Canadian Aeronautics and Space Journal. Le Journal Aéronautique et Spatial du Canada*, Vol. 36, No. 3, Sept. 1990, pp. 146–152.
[11] Chan, W. M., Rogers, S. E., Nash, S. M., Buning, P. G., and Meakin, R. L., "User's Manual for Chimera Grid Tools, Version 1.8," NASA Ames Research Center, May 2003.
[12] Chan, W. M., "The Overgrid Interface for Computational Simulations on Overset Grids," AIAA Paper 2002-3188, June 2002.
[13] Standish, K. J., "Aerodynamic Analysis of Blunt Trailing Edge Airfoils & a Microtab-Based Load Control System," M.S. Thesis, Univ. of California, Davis, Davis, CA, Dec. 2003.
[14] Standish, K. J., and van Dam, C. P., "Computational Analysis of a Microtab-Based Aerodynamic Load Control System for Rotor Blades," *Journal of the American Helicopter Society*, Vol. 50, No. 3, July 2005, pp. 249–258.
[15] *Operating Handbook for the UC Davis Low Turbulence Tunnel*, Aerolab, Laurel, MD, 1996.
[16] Drela, M., and Giles, M. B., "Viscous-Inviscid Analysis of Transonic and Low Reynolds Number Airfoils," *AIAA Journal*, Vol. 25, Oct. 1987, pp. 1347–1355.
[17] Barlow, J. B., Rae, W. H., Jr., and Pope, A., *Low-Speed Wind Tunnel Testing*, 3rd ed., John Wiley & Sons, Inc., New York, 1999.
[18] Michel, J., "Identification of the Aerodynamic Coefficients C_l, C_d and C_m of the GU25-5(11)8 and S809 Airfoils with Special Configurations," Research Project, Univ. of California, Davis, Davis, CA, 2001.
[19] Jones, B. M., "Measurement of Profile Drag by the Pitot-Traverse Method," Aeronautical Research Commission Reports and Memoranda No. 1688, 1936.
[20] Hopp, M., "Development and Application of an Automated Wake Analysis Method for Airfoils," M.S. Thesis, Univ. of California, Davis, Davis, CA, June 2002.
[21] Zayas, J., "UC Davis Wind Tunnel Automation and Airfoil Wake Base Analysis," M.S. Thesis, Univ. of California, Davis, Davis, CA, June 2002.
[22] Baker, J. P., "Experimental Investigation into the Effectiveness of a Microtab Aerodynamic Load Control System," M.S. Thesis, University of California, Davis, CA, June 2005.
[23] Somers, D. M., "Design and Experimental Results for the S809 Airfoil," NREL SR-440-6918, 1997.
[24] Braslow, A. L., and Knox, E. C., "Simplified Method for Determination of Critical Height Distributed Roughness Particles for Boundary-Layer Transition at Mach Numbers from 0 to 5," NACA TN 4363, Sept. 1958.
[25] Coleman, H. W., and Steele, W. G., *Experimentation and Uncertainty Analysis for Engineers*, John Wiley & Sons, Inc., New York, 1998.
[26] American Institute of Aeronautics and Astronautics, "Assessment of Experimental Uncertainty with Application to Wind Tunnel Testing," AIAA S-071A-1999.